# **RESEARCH PAPER**

# Comparative Anticancer Evaluation of Green and Chemically Synthesized MnO<sub>2</sub> Nanoparticles on Pancreatic Cancer Cells

Sarah F. AL Mayali <sup>1</sup>, Aula M. Al Hindawi <sup>1\*</sup>, Ibtihal Alshamarti <sup>2</sup>

#### ARTICLE INFO

# Article History: Received 25 June 2025 Accepted 28 September 2025 Published 01 October 2025

Keywords:
Anticancer
Flaxseed
MnO<sub>2</sub> NPs
Precipitation method

# **ABSTRACT**

Manganese dioxide (MnO<sub>2</sub>) nanoparticles were synthesized using two different methods: an environmentally friendly green synthesis using flaxseed extract as a natural reducing and stabilizing agent, and a conventional chemical precipitation method employing sodium thiosulfate (Na<sub>2</sub>S<sub>2</sub>O<sub>3</sub>·5H<sub>2</sub>O). Spectroscopic and structural characterization techniques (UV-Vis DRS, XRD, TEM, FESEM, EDX, and FTIR) revealed that the synthesis method significantly influenced the optical and structural properties of the nanoparticles. MnO2 nanoparticles obtained via green synthesis exhibited the β-MnO<sub>2</sub> phase and had a band gap energy of 1.57 eV, whereas those produced by the chemical method exhibited the  $\alpha$ -MnO<sub>2</sub> phase with a higher band gap of 2.06 eV. To assess their biological activity, cytotoxicity was evaluated against pancreatic cancer cells using the MTT assay. The results showed that both nanoparticle types caused a significant reduction in cell viability at high concentrations (500 µg/mL), while no significant cytotoxic effects were observed at lower concentrations (≤ 31.25 µg/mL). The IC<sub>50</sub> values indicated that the biosynthesized nanoparticles had greater cytotoxic potential (39.6 µg/mL) compared to the chemically synthesized ones (73.5 µg/mL), highlighting the influence of synthesis method on biological performance.

## How to cite this article

Mayali S., Hindawi A., Alshamarti I. Comparative Anticancer Evaluation of Green and Chemically Synthesized  $MnO_2$  Nanoparticles on Pancreatic Cancer Cells. J Nanostruct, 2025; 15(4):2319-2328. DOI: 10.22052/JNS.2025.04.070

## INTRODUCTION

Nanotechnology has brought major advancements to material science by allowing scientists to design materials with enhanced physical, chemical, and biological properties at the nanoscale [1]. One of the most promising nanomaterials in this field is manganese dioxide (MnO<sub>2</sub>), which has gained significant attention due to its unique crystalline structure [2, 3], redox behavior, and ability to respond to surface modifications. These features make

multiple valence states, and flexible structure. More recently, their potential in medical applications especially in cancer treatment [11, 12] has become a growing area of interest. Cancer creates a unique microenvironment in

MnO, nanoparticles useful in a wide range of

applications, such as electrochemical cells [4],

gas sensors [5], biosensors [6], energy storage

[7], catalysts [8], and environmental purification

[9, 10] due to their ability to exchange electrons,

<sup>&</sup>lt;sup>1</sup> Department of Chemistry, College of Education for Pure Sciences, University of Kerbala, kerbala, Iraq

<sup>&</sup>lt;sup>2</sup> Department of Basic Science, College of Dentistry, University of Kufa Najaf, Iraq

<sup>\*</sup> Corresponding Author Email: aula.m@uokerbala.edu.iq

the body that includes low oxygen levels [13], acidity, and high levels of certain chemicals like hydrogen peroxide [14]. These conditions offer an opportunity to use nanomaterials that respond specifically to the tumor environment. MnO<sub>2</sub> nanoparticles are particularly effective in this regard. In acidic and low-oxygen conditions, they can release oxygen and manganese ions, which helps reduce tumor hypoxia and improve the effectiveness of treatments like radiotherapy [15]. In addition, MnO, can produce reactive oxygen species (ROS)[16] that damage cancer cells by increasing oxidative stress, leading to programmed cell death through processes such as apoptosis and autophagy [17]. These nanoparticles can deliver chemotherapy drugs directly to the tumor site, where they are released in response to the tumor's internal conditions. This helps limit the damage to healthy cells and increases the drug's effectiveness. The way MnO<sub>2</sub> is synthesized plays a key role in its performance. Chemical methods like precipitation [18, 19], solgel [20], and hydrothermal [21] techniques are commonly used, but they can involve harmful substances and create toxic waste. As a safer alternative, green synthesis methods using plant extracts, microorganisms, or natural polymers are being explored. These environmentally friendly approaches often produce more biocompatible nanoparticles with larger surface areas and better functionality [22,23]. In cancer research, MnO<sub>3</sub> nanomaterials have shown promise not only in delivering drugs but also in improving imaging and boosting treatment responses by supplying oxygen to tumors. Their ability to combine diagnosis and therapy in a single platform makes them ideal candidates for modern cancer treatment approaches [24]. In this study, we investigate how different concentrations of MnO<sub>3</sub> nanoparticles affect the proliferation of pancreatic cancer cells. This will help to understand how these materials can be used as a treatment and how their effectiveness depends on the dose used on pancreatic cell.

## **MATERIALS AND METHOD**

Materials

Flaxseeds were obtained from a local supplier. Manganese sulfate (MnSO<sub>4</sub>·H<sub>2</sub>O, 99%) and sodium hydroxide were acquired from QualiKems Fine Chem and CDH, respectively. Sodium thiosulfate was supplied by Alpha Chemika. Deionized water served as the medium for the reactions.

Green synthesis

Preparation of Flaxseed Extract

After washing the flaxseeds with deionized water, they were allowed to dry at room temperature and then ground into a fine powder. Ten grams of flaxseed powder were mixed with 200 mL of deionized water and heated at 70 °C for 10 minutes with continuous stirring. The resulting mixture was then filtered using a porous cloth to separate the extract. The filtrate was used as a natural chelating agent for the preparation of manganese oxide nanoparticles.

# Synthesis of Manganese Dioxide Nanoparticles

Manganese dioxide nanoparticles (Flax-MnO<sub>2</sub>) were prepared using a green synthesis approach. A 0.01 M manganese sulfate solution was prepared by dissolving 0.0845 g of MnSO<sub>4</sub>. H<sub>2</sub>O in 50 mL of deionized water under continuous magnetic stirring at room temperature for 10 minutes. Sodium hydroxide solution was then gradually added to the mixture while stirring until the pH reached 11. After pH adjustment, 5 mL of the previously prepared flaxseed extract was added, and the mixture was heated at 70 °C for 2 hours under continuous stirring. The resulting precipitate was rinsed three times with deionized water to remove residual impurities, particularly sulfate ions. The solid product was separated by centrifugation at 4000 rpm for approximately 15 minutes. After centrifugation, the sample was washed again with deionized water and dried in a ceramic crucible at 100 °C for 1 hour using a drying oven. Finally, the dried material was finely ground using a mortar and calcined in a furnace at 400 °C for 2-3 hours.

# Chemical precipitation method

Preparation of Manganese Dioxide Nanoparticles

Manganese dioxide nanoparticles (Thio-MnO<sub>2</sub>) were synthesized through a chemical precipitation method, involving manganese sulfate and sodium thiosulfate as precursors. Initially, a solution of MnSO<sub>4</sub>.H<sub>2</sub>O (0.02 M) was prepared in deionized water under continuous magnetic stirring. A freshly prepared sodium thiosulfate solution (0.01 M) was then added gradually to the manganese sulfate solution while maintaining constant stirring at ambient or slightly elevated temperatures (around 70-80 °C). Sodium thiosulfate functioned

> J Nanostruct 15(4): 2319-2328, Autumn 2025 (cc) BY

both as a reducing and stabilizing agent, promoting the formation of  $\rm MnO_2$  nanoparticles. The appearance of a dark brown or black precipitate indicated successful synthesis. The resulting solid was separated by centrifugation, thoroughly washed with deionized water to eliminate residual impurities, and then dried at 80–100 °C for 60 minutes. For enhanced crystallinity, the dried material was optionally calcined at 400 °C for three hours.

Detection viability pancreatic cancer cells with MnO,

Tissue culture

PANC-1 cells represent a model of human pancreatic ductal adenocarcinom. These cells were cultured in RPMI-1640 medium supplemented with 10% fetal bovine serum (FBS), 100 units/mL penicillin, and 100  $\mu$ g/mL streptomycin. The cells were passaged at 80% confluence using Trypsin-EDTA solution, and passaging was performed twice weekly at 37°C.

# Viability assay (MTT)

The cytotoxicity of manganese dioxide nanoparticles was evaluated using an MTT assay to assess proliferation cancer cells. Cells were cultured in 96-well plates at a concentration of  $1\times$ 

10<sup>4</sup> cells per well. After 24 hours, a homogeneous monolayer was formed, and the cells were treated with medium containing different concentrations of prepared MnO $_2$  NPs for testing (500, 250, 125, 62.5, 31.25, and 15.62 µg/mL). The test was conducted with the same concentrations for both types of MnO $_2$  NPs: one prepared by the green method using flaxseed extract as a reducing agent, and the other by the precipitation method using Na $_2$ S,O $_3$  as a chemical reducing agent.

Next, 28  $\mu$ L of 2 mg/mL MTT solution was added, and the cells were incubated for 2.5 hours. Cell viability was assessed 72 hours after treatment at 37°C. After removing the MTT solution, 130  $\mu$ L of 1% DMSO was added to dissolve the formazan crystals, and the plates were incubated for 15 minutes at 37°C with gentle shaking. Absorbance was measured at 492 nm using a microplate reader, and the test was performed in triplicate for confirmation. Cytotoxicity was calculated using the following equation:

% Cytotoxicity = 
$$\frac{A-B}{A}$$
 x 100 (1)

# Characterization

A range of characterization techniques was employed to examine the physicochemical

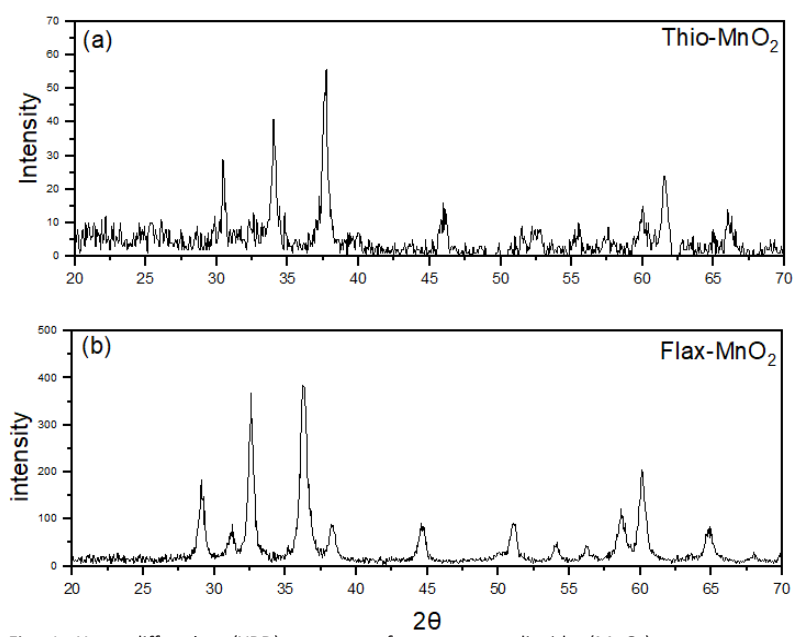


Fig. 1. X-ray diffraction (XRD) patterns of manganese dioxide (MnO $_2$ ) nanostructures synthesized using.

the synthesized properties nanostructures. The optical behavior of the manganese dioxide was analyzed using a UV-1800 Shimadzu spectrophotometer (Japan). To identify the functional groups present in the flaxseed extract and to confirm the formation of MnO<sub>2</sub>, Fourier Transform Infrared Spectroscopy (FT-IR, SHIMADZU) was utilized. Additionally, X-ray diffraction (XRD) patterns were obtained using CuK $\alpha$  radiation ( $\lambda$  = 0.154056 nm) over a scanning range of 20° to 70°, to investigate the crystalline structure of the samples. Electron microscopies (TEM and FESEM) were used to study the structural properties of the prepared particles. Energy-Dispersive X-ray Spectroscopy (EDX) was utilized to examine the elemental composition of MnO<sub>2</sub> nanoparticles synthesized through both green (plant extract) and conventional chemical precipitation methods.

#### **RESULTS AND DISCUSSION**

XRD analysis offers essential information on the crystal structure and phase purity of the produced MnO, nanoparticles. In this study, the XRD results verified that the nanoparticles exhibit a distinct crystalline lattice, with diffraction peaks corresponding to the characteristic MnO<sub>3</sub> planes as indexed in the Joint Committee on Powder Diffraction Standards (JCPDS) database. As seen in Fig. 1a, the XRD analysis of MnO<sub>3</sub> sample prepared by chemical precipitation method showed distinct, sharp diffraction peaks at 2θ values of 29.1°, 32.6°, 36.2°, 44.5°, 51.1°, 60.2°, and 64.7°, corresponding to the (310), (102), (110), (101), (411), (521) and (002) crystallographic planes, respectively. These reflections match JCPDS card No. (044-0141), confirming the formation of the  $\alpha$ - MnO<sub>3</sub> phase

with a tetragonal lattice [25]. The crystallite size for the (110) plane was estimated by the Debye–Scherrer equation [26], yielding an average value of ~9.12 nm.

For the MnO<sub>2</sub> synthesized via the green method, the XRD pattern in Fig. 1b revealed diffraction peaks indicative of a tetragonal lattice with beta phase. However, a notable shift in peak positions was observed compared to the Thio-MnO<sub>2</sub> pattern. This variation in peak position and intensity underscores the influence of plant-derived bioactive compounds on MnO<sub>2</sub> crystallization and nanoparticle growth. These findings are consistent with earlier literature. The average crystallite size was estimated to be approximately 14.63 nm using the Debye–Scherrer equation.

The optical properties of MnO<sub>2</sub> nanostructures were investigated using Diffuse Reflectance Spectroscopy (DRS). It is clear from Fig. 2 that the UV-DRS spectra of both samples showed significant absorption in the visible light region, suggesting their effectiveness in capturing a wide portion of the solar spectrum. The reflectance values were transformed using the Kubelka–Munk function:

$$(F(R)h\upsilon)^{n} = k (h\upsilon - Eg)$$
 (2)

Where F(R) represents the Kubelka–Munk function associated with absorbance, n denotes the type of electronic transition (indirect allowed transitions) [27], h is Planck's constant, k is a proportionality constant, and  $\upsilon$  is the frequency of the incident light. By plotting  $(F(R)h\upsilon)^{1/2}$  against photon energy, the band gap energy  $(E_g)$  can be estimated by extrapolating the linear portion of the curve to intersect the photon energy (x-axis).

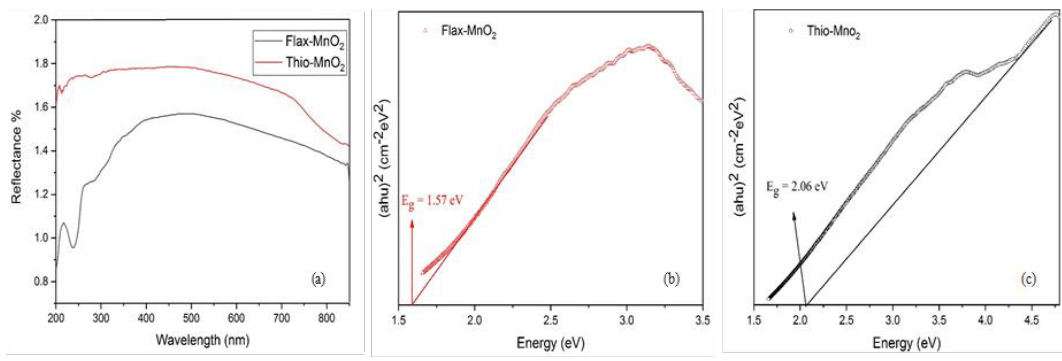


Fig. 2. UV-DRS spectra of Flax-MnO<sub>2</sub> and Thio-MnO<sub>2</sub> nanoparticles (a), along with the corresponding estimated band gap energies for Flax-MnO<sub>3</sub> (b) and Thio-MnO<sub>3</sub> (c).

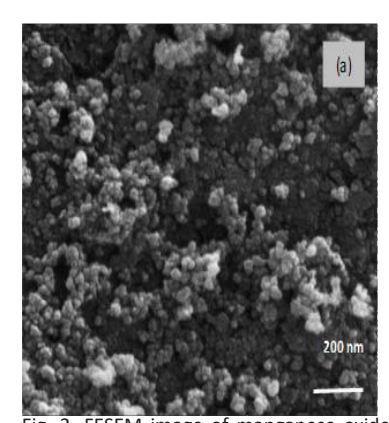
Based on the analysis using the Kubelka–Munk function, the estimated optical band gap energies of Flax-MnO $_2$  and Thio-MnO $_2$  were approximately 1.57 eV and 2.06 eV, respectively. It is important to note that the optical band gap is strongly influenced by the crystalline structure of the synthesized semiconductors. According to the XRD results, the MnO $_2$  nanostructures synthesized in the presence of flaxseeds could exhibit a  $\beta$ -phase structure. The estimated band gap value of 1.57 eV falls within or slightly above the commonly reported range for  $\beta$ -MnO $_2$  (~0.25–1.3 eV) [28], which is attributed to its compact crystalline structure that promotes enhanced orbital overlap and consequently reduces the band gap energy.

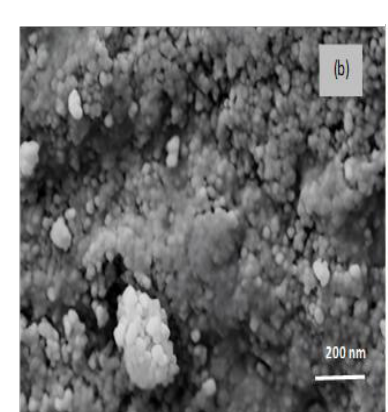
 $\text{MnO}_2$  nanoparticles synthesized in the presence of sodium thiosulfate exhibited a band gap energy of approximately 2.06 eV, which aligns well with values reported in the literature (typically ranging from 1.7 to 2.6 eV), suggesting alpha phase [28, 29]. The  $\alpha\text{-MnO}_2$  particles are characterized by a tunnel-type crystal structure, formed by the connection of  $\text{MnO}_2$  octahedra into large 2×2 and 1×1 tunnels [29-31]. This open framework can host various cations and significantly affects the material's electronic structure. Consequently,  $\alpha\text{-MnO}_2$  generally displays a wider band gap compared to its more compact polymorphs.

To compare the surface morphology of  $\mathrm{MnO}_2$  nanoparticles synthesized via the plant extract method and chemical precipitation, field-emission scanning electron microscopy (FESEM) was used. As can be seen from the images in Fig. 3a and b that both prepared nanoparticles are spherical and quasi-spherical shapes, with some degree

of agglomeration observed in localized clusters especially with chemical route. The EDX spectra of both samples prominently displayed peaks corresponding to manganese (Mn) and oxygen (O), confirming the successful formation of manganese dioxide. In both techniques, the synthesized MnO<sub>2</sub> exhibited a clean EDX spectrum with minimal impurities, indicating relatively high material purity (see Fig. 3c). Distinct signals for gold (Au) were also observed in both spectra, likely due to the thin gold coating applied to the sample surface to enhance electrical conductivity during Field Emission Scanning Electron Microscopy (FESEM) imaging [32, 33].

Fig. 4a shows the TEM image of Flax-MnO<sub>3</sub> nanoparticles, these particles are relatively uniform, and quasi-spherical shapes with mild agglomeration due to the presence of residual organic compounds in the plant extract, which may act as capping agents. These biomolecules help stabilize the particles but can also cause slight particle adhesion [34] Conversely, Thio-MnO<sub>2</sub> nanoparticles appeared more dispersed and welldefined, with sharper edges and a smaller average size, as shown in Fig. 4b. This morphological difference is attributed to the absence of organic stabilizers in the chemical synthesis process, which allows for more precise control over nucleation and crystal growth. These findings highlight the critical role of the synthesis approach in determining the structural and morphological properties of MnO<sub>3</sub> nanostructures. The average particle sizes were estimated using ImageJ software and they found to be approximately 22 ± 2.6 nm for the greensynthesized MnO<sub>3</sub> and 17 ± 3.1 nm for those





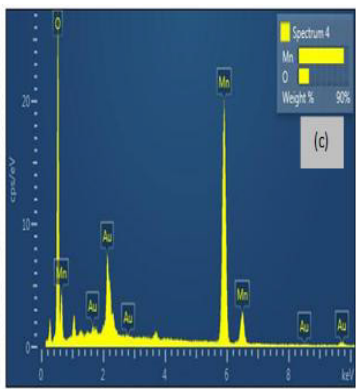


Fig. 3. FESEM image of manganese oxide (MnO<sub>2</sub>) nanoparticles synthesized by green method using flaxseed extract (a) and chemical precipitation method using sodium thiosulfate (b). The scale bars for these images are 200 nm. EDX for Flax-MnO<sub>2</sub> nanoparticles(c).

prepared via chemical precipitation.

The FTIR spectra of Flax-MnO<sub>2</sub> and Thio-MnO<sub>2</sub> were recorded in the range of 500-4000 cm<sup>-1</sup> as shown in Fig. 5a and b. Two absorption peaks appear at 517 and 614 cm<sup>-1</sup>, are assigned to Mn–O stretching vibrations bond [35], indicating the formation of MnO<sub>2</sub>. However, no peak was observed in that region in the spectrum of flaxseeds (Fig. 5c). Other peaks observed in the spectrum of Flax-MnO<sub>2</sub> at 1240 cm<sup>-1</sup> and 1777 cm<sup>-1</sup> are attributed to C–O and C–H bonds, respectively, resulting from the active components in the extract (such as flavonoids) [36]. These peaks remained apparent despite the sample being exposed to a high calcination temperature (400

°C), indicating that some organic compounds remained as a coating on the surface of the prepared particles [37]. A broad absorption peak was also observed at 3409 cm<sup>-1</sup>, attributed to the -OH group stretching vibrations and H–O–H bending of water molecules, likely resulting from the sample's absorption of moisture. In addition, a modest absorption peak appeared at 1626 cm<sup>-1</sup> due to the bending of water molecules. A strong peak centered at ~1116 cm<sup>-1</sup> is assigned to S–O or S=O bond stretching, which is possibly related to sodium thiosulfate residues used in the reduction process.

Viability of pancreatic cancer cell lines treated with MnO<sub>2</sub> nanoparticles synthesized from

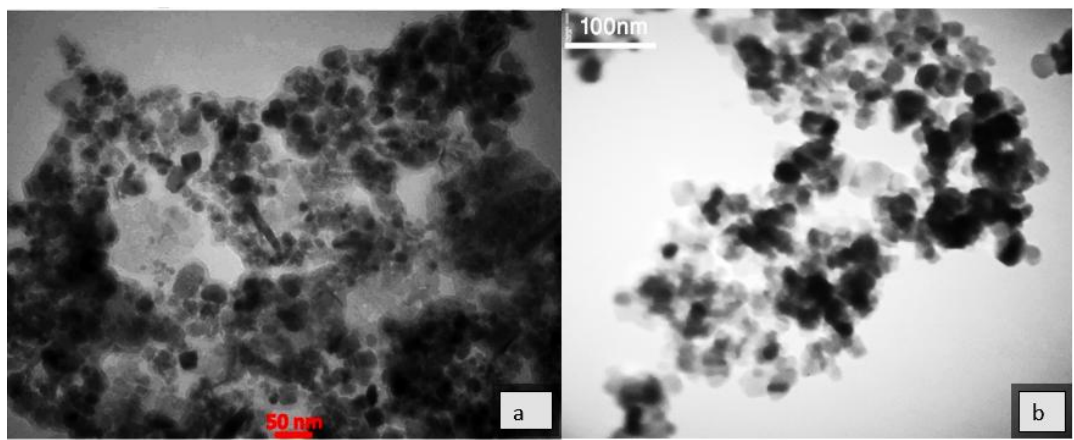


Fig. 4. TEM images of the prepared manganese dioxide nanostructures in the presence of flax seeds extract (a), and in the presence of sodium thiosulfate (b).

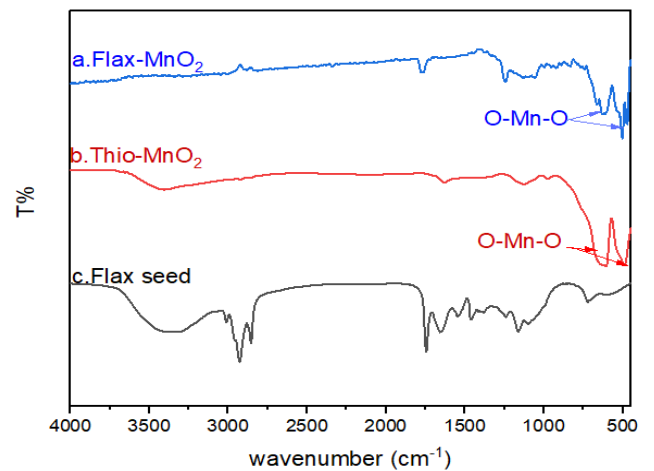


Fig. 5. FTIR of Manganese dioxide nanostructure prepared using flax seeds (a), Manganese dioxide nanostructure prepared using sodium thiosulfate (b) flax seeds powder (c).

Flaxseed. The cytotoxic activity of the synthesized  $MnO_2$  nanoparticles against pancreatic cancer cell lines was evaluated using the MTT assay at various concentrations. The results showed that a high concentration (500 µg/mL) significantly reduced cell viability, with only 11% viability remaining compared to the control group, as illustrated in Fig. 6. This demonstrates that  $MnO_2$  nanoparticles at this concentration exhibit strong cytotoxic effects on cancer cells, causing a statistically significant decrease in cell proliferation (p < 0.001).

Similar results were observed in a previous study where breast cancer cells (MDA-MB-231) treated with nanoparticles showed reduced proliferation after 24 hours compared to the control group [38]. Conversely, at lower concentrations particularly below 31.25  $\mu$ g/mL the MnO<sub>2</sub> nanoparticles exhibited no significant cytotoxic effect on the pancreatic cancer cell lines compared to the control group. This inverse relationship between MnO<sub>2</sub>

concentration and cell viability is noteworthy: as the concentration of  $MnO_2$  decreases, the relative viability of pancreatic cancer cells increases.

This type of experiment is a standard approach for determining the toxicological profile of  $MnO_2$  nanoparticles on cancer cells. It plays a crucial role in identifying concentration thresholds at which  $MnO_2$  becomes toxic or is considered safe, potentially without adverse effects.

The next step is done by using Thio-MnO<sub>2</sub> nanoparticles to evaluate nanoparticles in cytotoxic effect of pancreatic cancer cells: Pancreatic cancer cells were treated with different concentrations of the nanoparticles between (7.8 to 500 ug/ml) except control group (untreated cells). The results showed that a high Concentration (500 ug/ml) is significantly low viability of pancreatic cell, so it indicated the strong cytotoxic effect on cell proliferation. While 125 ug/ml is recorded 30%. On other hand, lower concentrations (7.8

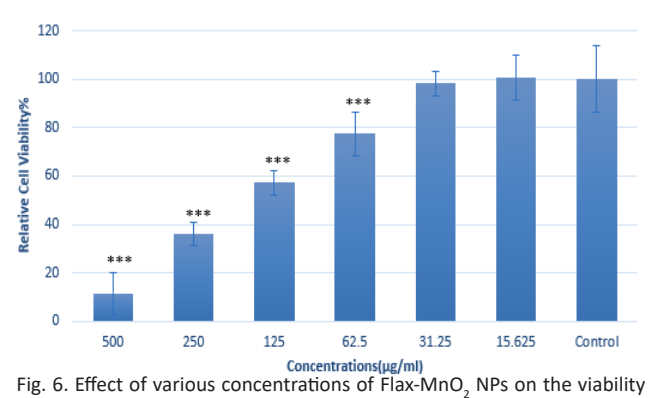


Fig. 6. Effect of various concentrations of Flax-MnO<sub>2</sub> NPs on the viability of pancreatic cancer cells.

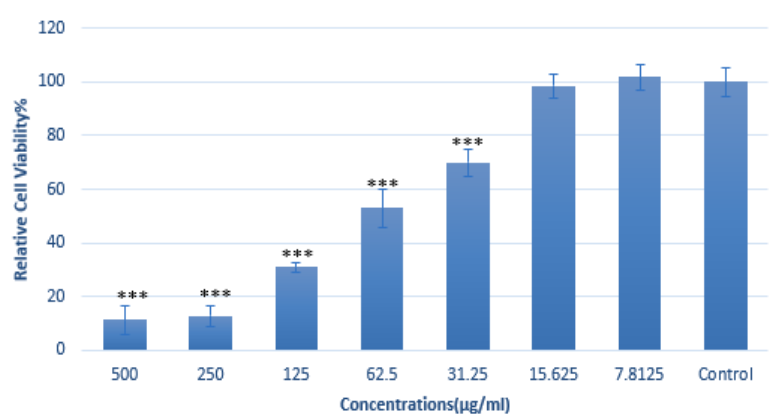


Fig. 7. Effect of various concentrations of Thio-MnO<sub>2</sub> NPs on the viability of pancreatic cancer cells.

ug/ml and 15.6 ug/ml), the MTT is nearly similar to control group (100%). It noted that toxicity no significant effect on cancer cell, as shown in Fig. 7. The most surprising aspect of the data is that the no observed effect concentration (NOEC) is between 7.8125 and 15.625 ug/ml, while lowest observed effect concentration (LOEC) is recorded 31.25 ug/ml in contrast to control group.

This is critical for biological and biomedical applications where the material  $(MnO_2)$  will be used directly with cells to design a new products of drug [39, 40].

## IC50 (Half Maximal Inhibitory Concentration)

The IC50 value was measured to determine the potency of MnO<sub>2</sub> nanoparticles in inhibiting cancer cell viability, specifically identifying the concentration needed to reduce cell viability by

50%. The findings indicated that the IC50 of  $MnO_2$  nanoparticles was 39.6 µg/mL, meaning that this concentration is expected to reduce cell viability by 50% relative to the untreated control group, take a look at Fig. 8. This information is considered fundamental in the fields of drug discovery and toxicology, as it provides essential insights into the efficacy and safety of potential therapeutic compounds [41].

Half Maximal Inhibitory Concentration ( $IC_{50}$ ) was done to detect the  $MnO_2$  nanoparticles from  $Na_2S_2O_3.5H_2O$  impact on pancreatic cancer cell and the best concentration that required to reduce viability these cells . The results showed that Interpretation of  $IC_{50}$  was 73.5 ug/ml of the  $MnO_2$  is expected to cause a 50% reduction in cell viability compared to the control group, look at Fig. 9.

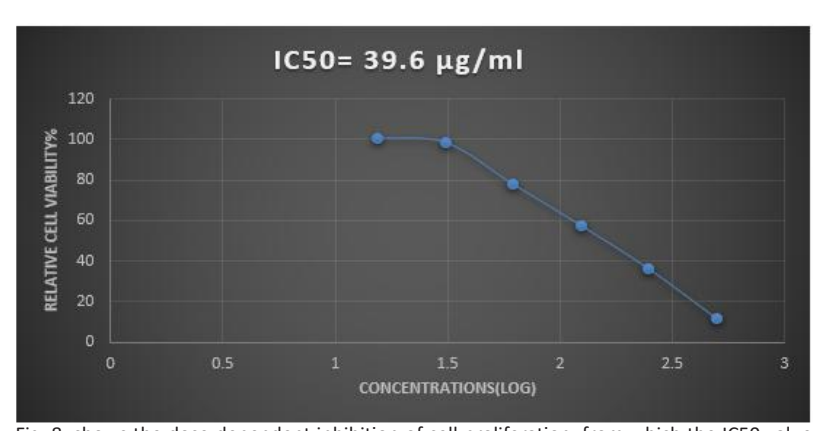
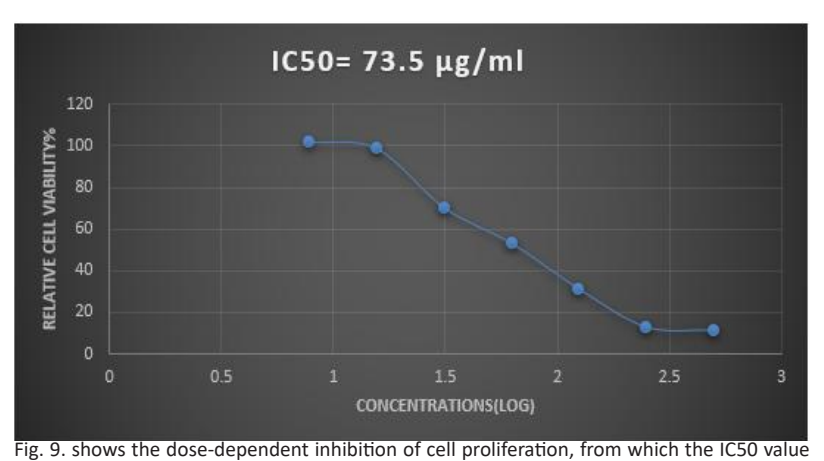


Fig. 8. shows the dose-dependent inhibition of cell proliferation, from which the IC50 value was calculated using nonlinear regression analysis for Flax-MnO<sub>2</sub>.



was calculated using nonlinear regression analysis for Thio-MnO<sub>2</sub>.

#### **CONCLUSION**

This study focused on the preparation and characterization of manganese dioxide (MnO<sub>2</sub>) nanoparticles using two different methods: a green synthesis method and a chemical precipitation method. The results revealed that the optical band gap was approximately 1.7 eV for the β-MnO₂ phase (green method) and 2.06 eV for the α-MnO<sub>2</sub> phase (chemical method), indicating that the optical properties are influenced by both the crystal phase and the synthesis approach. Morphological analyses (FESEM, TEM) showed that nanoparticles produced via the green method were nearly spherical with some degree of agglomeration, whereas those synthesized chemically were smaller and more uniform in shape.

The cytotoxic activity of the green-synthesized nanoparticles against pancreatic cancer cells demonstrated a significant inhibitory effect at high concentrations (500  $\mu$ g/mL), while lower concentrations had minimal or no effect. The IC<sub>50</sub> value was determined to be 39.6  $\mu$ g/mL, suggesting that these particles could serve as promising candidates for pancreatic cancer treatment, provided their concentrations are carefully controlled. Similarly, the chemically synthesized nanoparticles exhibited cytotoxic effects at high concentrations, with an IC<sub>50</sub> value of 73.5  $\mu$ g/mL, and showed no significant toxicity at lower doses.

# **CONFLICT OF INTEREST**

The authors declare that there is no conflict of interests regarding the publication of this manuscript.

### **REFERENCES**

- Pawar K, Kachave R, Kanawade M, Zagre V. A Review on Nanoparticles Drug Delivery System. Journal of Drug Delivery and Therapeutics. 2021;11(4):101-104.
- Abuzeid HM, Julien CM, Zhu L, Hashem AM. Green Synthesis of Nanoparticles and Their Energy Storage, Environmental, and Biomedical Applications. Crystals. 2023;13(11):1576.
- 3. Wang F, Zheng Y, Chen Q, Yan Z, Lan D, Lester E, et al. A critical review of facets and defects in different MnO2 crystalline phases and controlled synthesis Its properties and applications in the energy field. Coordination Chemistry Reviews. 2024;500:215537.
- 4. Yang S, Feng C, Spence D, Al Hindawi AMAA, Latimer E, Ellis AM, et al. Robust Ferromagnetism of Chromium Nanoparticles Formed in Superfluid Helium. Advanced Materials. 2016;29(1).
- Singh A, Verma A, Yadav BC. MnO<sub>2</sub>-SnO<sub>2</sub> Based Liquefied Petroleum Gas Sensing Device for Lowest Explosion Limit

- Gas Concentration. ECS Sensors Plus. 2022;1(2):025201.
- Hao L, Xue L, Huang F, Cai G, Qi W, Zhang M, et al. A Microfluidic Biosensor Based on Magnetic Nanoparticle Separation, Quantum Dots Labeling and MnO<sub>2</sub> Nanoflower Amplification for Rapid and Sensitive Detection of Salmonella Typhimurium. Micromachines. 2020;11(3):281.
- Shin J, Seo JK, Yaylian R, Huang A, Meng YS. A review on mechanistic understanding of MnO<sub>2</sub> in aqueous electrolyte for electrical energy storage systems. International Materials Reviews. 2019;65(6):356-387.
- Hraja M, Al Hindawi A, Shiltagh N. Investigation of Electronic and Molecular Features of Zn3S3/PEG4000 Nano-Composite Using the DFT Method. Journal of the Turkish Chemical Society Section A: Chemistry. 2024;11(2):565-574.
- Yang R, Fan Y, Ye R, Tang Y, Cao X, Yin Z, et al. MnO<sub>2</sub>-Based Materials for Environmental Applications. Advanced Materials. 2021;33(9).
- 10. Lu H, Zhang X, Khan SA, Li W, Wan L. Biogenic Synthesis of MnO<sub>2</sub> Nanoparticles With Leaf Extract of Viola betonicifolia for Enhanced Antioxidant, Antimicrobial, Cytotoxic, and Biocompatible Applications. Frontiers in Microbiology. 2021-12
- Yang G, Ji J, Liu Z. Multifunctional MnO<sub>2</sub> nanoparticles for tumor microenvironment modulation and cancer therapy. WIREs Nanomedicine and Nanobiotechnology. 2021;13(6).
- Xia H-Y, Li B-Y, Zhao Y, Han Y-H, Wang S-B, Chen A-Z, et al. Nanoarchitectured manganese dioxide (MnO2)-based assemblies for biomedicine. Coordination Chemistry Reviews. 2022;464:214540.
- Chen Z, Han F, Du Y, Shi H, Zhou W. Hypoxic microenvironment in cancer: molecular mechanisms and therapeutic interventions. Signal Transduction and Targeted Therapy. 2023;8(1).
- Zaher A, Petronek MS, Allen BG, Mapuskar KA. Balanced Duality: H<sub>2</sub>O<sub>2</sub>-Based Therapy in Cancer and Its Protective Effects on Non-Malignant Tissues. International Journal of Molecular Sciences. 2024;25(16):8885.
- 15. Decision letter for "Hollow nanosystem-boosting synergistic effect between photothermal therapy and chemodynamic therapy via self-supplied hydrogen peroxide and relieved hypoxia". Royal Society of Chemistry (RSC); 2024.
- 16. Xu X, Duan J, Liu Y, Kuang Y, Duan J, Liao T, et al. Multistimuli responsive hollow MnO<sub>2</sub>-based drug delivery system for magnetic resonance imaging and combined chemo-chemodynamic cancer therapy. Acta Biomaterialia. 2021;126:445-462.
- Greene A, Hashemi J, Kang Y. Development of MnO<sub>2</sub> hollow nanoparticles for potential drug delivery applications. Nanotechnology. 2020;32(2):025713.
- Turki ZT, Hindawi AMA, Shiltagh NM. Fabrication and characterization of cadmium sulfide nanoparticles using chemical precipitation method. AIP Conference Proceedings: AIP Publishing; 2023. p. 030008.
- Ali Hamzah H, Al Hindawi AM, Al-Qaim FF. Green Synthesis of Tin Oxide Nanoparticles for the Removal of Mefenamic Acid from Aqueous Solutions. Lecture Notes in Networks and Systems: Springer Nature Singapore; 2025. p. 569-581.
- Reddy RN, Reddy RG. Sol–gel MnO<sub>2</sub> as an electrode material for electrochemical capacitors. Journal of Power Sources. 2003;124(1):330-337.
- Dawadi S, Gupta A, Khatri M, Budhathoki B, Lamichhane G, Parajuli N. Manganese dioxide nanoparticles: synthesis, application and challenges. Bulletin of Materials Science. 2020;43(1).

J Nanostruct 15(4): 2319-2328, Autumn 2025

- 22. Kalimuthu K, Cha BS, Kim S, Park KS. Eco-friendly synthesis and biomedical applications of gold nanoparticles: A review. Microchemical Journal. 2020;152:104296.
- 23. Bhardwaj B, Singh P, Kumar A, Kumar S, Budhwar V. Eco-Friendly Greener Synthesis of Nanoparticles. Advanced Pharmaceutical Bulletin. 2020;10(4):566-576.
- 24. Xu Y, Tan W, Chen M, Chen S, Tang K, Liao H, et al. MnO<sub>2</sub> coated multi-layer nanoplatform for enhanced sonodynamic therapy and MR imaging of breast cancer. Frontiers in Bioengineering and Biotechnology. 2022;10.
- Yadav S, x S, Phogat P, Jha R, Singh S. Preparation of Tin Oxide Nanoparticles via Co-Precipitation Method for its Future Applications. International Journal of Science and Research (IJSR). 2024;13(6):1302-1306.
- 26. Al Hindawi, A. M., Abd Al-Aama, Z. M., Al-Sabbagh, J. K., & Awad, M. (2025). Zinc oxide nanoparticles: An experimental study of synthesis, characterization and biological activity. Journal of the Serbian Chemical Society. 90(1:, 27-37.
- Cockayne E, Li L. First-principles DFT + U studies of the atomic, electronic, and magnetic structure of α-MnO<sub>2</sub> (cryptomelane). Chemical Physics Letters. 2012;544:53-58.
- Devi R, Kumar V, Kumar S, Bulla M, Sharma S, Sharma A. Electrochemical Analysis of MnO<sub>2</sub> (α, β, and γ)-Based Electrode for High-Performance Supercapacitor Application. Applied Sciences. 2023;13(13):7907.
- 29. Gangwar D, Rath C. Structural, optical and magnetic properties of  $\alpha$  and  $\beta$ -MnO $_2$  nanorods. Applied Surface Science. 2021;557:149693.
- Song J, Liu M, Ma X, Tian Q, Feng J, Zhong X, et al. Thermal decomposition behavior and computational analysis of alpha and beta manganese dioxide nanorods. Journal of Alloys and Compounds. 2023;962:171208.
- 31. Shehroz H, Ali S, Bibi G, Khan T, Jamil S, Khan SR, et al. Comparative investigation of the catalytic application

- of  $\alpha/\beta/\gamma$ -MnO  $_2$  nanoparticles synthesized by green and chemical approaches. Environmental Technology. 2022;45(6):1081-1091.
- 32. Tukko MN, Al-hajji MA, Alasle S, Al-Okla M, Zeidan H. Impact of Temperature on the Structural and Optical Properties of Silver Sulfide Films Prepared by Chemical Bath Deposition. Elsevier BV; 2024.
- 33. Ahmed, A., Al Hindawi, A., & Shiltagh, N. (2024). Role of manganese ion in tuning the structural and optical properties of silver sulfide nanostructures. Chemical Review and Letters. 7(4); 622-629.
- 34. Morteza Naghib S, Garshasbi HR. Green Synthesis and Antibacterial Activity of Noble Metal Nanoparticles using Plants. Green Plant Extract-Based Synthesis of Multifunctional Nanoparticles and their Biological Activities: BENTHAM SCIENCE PUBLISHERS; 2023. p. 1-29.
- Al Hindawi AM, Joudah I, Hamzah S, Tarek Z. Plant extract: safe way for fabrication silver nanoparticles. IOP Conference Series: Materials Science and Engineering. 2019;571(1):012069.
- Turki, Z. T., Al Hindawi, A. M., & Shiltagh, N. M. (2022).
   Green synthesis of CdS nanoparticles using avocado peel extract. NanoWorld Journal. 8:73-78.
- S.Ganeshan, P.Ramasundari, A.Elangovan, G.Arivazhagan, R.Vijayalakshmi. Synthesis and Characterization of MnO<sub>2</sub> Nanoparticles: Study of Structural and Optical Properties. International Journal of Scientific Research in Physics and Applied Sciences. 2017;5(6):5-8.
- Jaganyi D, Altaf M, Wekesa I. Synthesis and characterization of whisker-shaped MnO<sub>2</sub> nanostructure at room temperature. Applied Nanoscience. 2012;3(4):329-333.
- Szewczyk OK, Roszczenko P, Czarnomysy R, Bielawska A, Bielawski K. An Overview of the Importance of Transition-Metal Nanoparticles in Cancer Research. International

(CO) BY